Investigating Salinity Effect on Temperate Coastal Wetland Soil Microbes and Greenhouse Gas Emissions.

Emilia Chiapponi[1], Denis Zannoni[1], Beatrice Maria Sole Giambastiani[2], Sonia Silvestri[1], Alessandro Buscaroli[1], and Federica Costantini[1]

[1]University of Bologna
[2]BIGEA - Biological, Geological, and Environmental Sciences, University of Bologna

April 29, 2024

Abstract

Coastal wetlands capture carbon dioxide from the atmosphere at high rates and store large amounts of "blue carbon" in soils. These habitats are home to a variety of microbial communities that break down organic matter and cycle nutrients, playing a substantial role in coastal biogeochemical balance. Rising sea levels make coastal wetlands more susceptible to saltwater intrusion, which might disrupt biogeochemical processes, such as the sulfur cycle and methane generation/consumption by bacteria thus disrupting existing equilibria. A change in biogeochemical equilibria may produce important climate-related feedback because these systems, while involved in carbon sequestration, also have the potential to emit greenhouse gases, with reported higher emissions in freshwater ecosystems compared to brackish ones. In this study, we characterize the microbial community and geochemical properties in soils of three temperate coastal wetlands along a salinity gradient to assess the effect of salinity on organic matter decomposition and related greenhouse gas emissions. The full-length Oxford Nanopore MinION 16S rRNA amplicon sequencing is used to characterize bacterial communities from soil samples. Results indicate a prevalence of sulfur-reducing bacteria in salinized sites compared to freshwater sites. In brackish environments, there is an emergence of obligate anaerobic taxa associated with sulfate reduction, fatty acid degradation, and denitrifying bacteria. These microbial communities play a significant role in reducing CH4 emissions while simultaneously increasing CO2 emissions within these habitats. This study reveals the structure of microbial communities in wetland soils, crucial for ecosystem understanding and implications in wetland conservation, management, and climate change mitigation.

Hosted file

`manuscript_draft - EC16_final.docx` available at https://authorea.com/users/770503/articles/843443-investigating-salinity-effect-on-temperate-coastal-wetland-soil-microbes-and-greenhouse-gas-emissions

AGU PUBLICATIONS

Investigating Salinity Effect on Temperate Coastal Wetland Soil Microbes and Greenhouse Gas Emissions.

Emilia Chiapponi[1], Denis Zannoni[1], Beatrice Maria Sole Giambastiani[1], Sonia Silvestri[1], Alessandro Buscaroli[1], Federica Costantini[1]

[1]Biological, Geological and Environmental Sciences Department, University of Bologna, Ravenna Campus, Italy

Corresponding Author: Emilia Chiapponi (emilia.chiapponi2@unibo.it)

Key Points:

1. Sulfur-oxidizing bacteria dominated in freshwater, with sulfate-reducers thrived in brackish areas, indicating salinity-driven shifts.
2. Brackish waters foster sulfate-reducing bacteria, resulting in lower CH_4 emissions than freshwater settings.
3. Salinity reduces CH4 emissions, suggesting a trade-off between lower CH4 and higher CO2 emissions with rising salinity.

ABSTRACT

Coastal wetlands capture carbon dioxide from the atmosphere at high rates and store large amounts of “blue carbon” in soils. These habitats are home to a variety of microbial communities that break down organic matter and cycle nutrients, playing a substantial role in coastal biogeochemical balance. Rising sea levels make coastal wetlands more susceptible to saltwater intrusion, which might disrupt biogeochemical processes, such as the sulfur cycle and methane generation/consumption by bacteria thus disrupting existing equilibria. A change in biogeochemical equilibria may produce important climate-related feedback because these systems, while involved in carbon sequestration, also have the potential to emit greenhouse gases, with reported higher emissions in freshwater ecosystems compared to brackish ones. In this study, we characterize the microbial community and geochemical properties in soils of three temperate coastal wetlands along a salinity gradient to assess the effect of salinity on organic matter decomposition and related greenhouse gas emissions. The full-length Oxford Nanopore MinION 16S rRNA amplicon sequencing is used to characterize bacterial communities from soil samples. Results indicate a prevalence of sulfur-reducing bacteria in salinized sites compared to freshwater sites. In brackish environments, there is an emergence of obligate anaerobic taxa associated with sulfate reduction, fatty acid degradation, and denitrifying bacteria. These microbial communities play a significant role in reducing CH_4 emissions while simultaneously increasing CO_2 emissions within these habitats. This study reveals the structure of microbial communities in wetland soils, crucial for ecosystem understanding and implications in wetland conservation, management, and climate change mitigation.

Plain Language Summary

Coastal wetlands are important habitats that help to regulate the global carbon cycle. Microbial communities in these wetland soils break down organic matter and cycle nutrients but also produce greenhouse gas emissions. In this study, we investigate the microbial communities in three different temperate coastal wetland soils along a salinity gradient, from saline to freshwater systems. We found that the differences in microbes involved in the carbon cycle among sites are mainly driven by salinity. In environments with higher salinities, microbial communities were contributing to a reduction in CH_4 production but were producing

more CO_2. The results suggest that biogeochemical studies in wetlands are important for understanding climate feedbacks involving these ecosystems and mitigating climate change through carbon sequestration. Moreover, the study evidenced how it is important to characterize the microbial communities in wetland soils, which is critical for understanding ecosystem processes with substantial implications for wetland conservation and management.

1. Introduction

Coastal vegetated wetlands are transitional ecosystems found at the edge of terrestrial and marine habitats (Mitsch et al., 2013). The amount of carbon, also defined as "blue carbon", stored in coastal wetland soils is estimated to equal 25 Pg at the global scale (Duarte et al., 2013) and comes from a constant sink of organic matter associated with slow rates of decomposition. Coastal wetlands are among the most efficient ecosystems in terms of carbon sequestration rate, storing 67–215 Tg C yr^{-1} (Hopkinson et al., 2012), thus playing a crucial role in global biogeochemical cycles (IPCC, 2022). Wetland soils are home to diverse microbial communities that are responsible for driving the processes of organic matter breakdown, nutrient cycling, and greenhouse gas emissions (Bridgham et al., 2013). The elements that drive microbial metabolism, such as temperature and precipitation, local environmental characteristics like vegetation, hydrology and soil type, and land use (undisturbed vs. disturbed), influence the rates at which organic carbon mineralizes (Bonetti et al., 2021).

Coastal wetlands are increasingly vulnerable to saltwater intrusion due to sea level rises (White and Kaplan, 2017) and this might reduce the amount of carbon that they can sequester through vegetation and microbial communities disrupting biogeochemical cycles (Morrissey et al., 2014; Dang et al., 2019). Methanogenic, fermentative, and respiratory pathways are only a few of the many bacterial metabolic activities that drive the complex processes of organic matter breakdown in these environments (Liang et al., 2023). Due to the restricted availability of terminal electron acceptors, methanogenesis is more prevalent in freshwater settings whereas sulfate reduction is prevalent in coastal saltwater systems (Poffenbarger et al., 2011).

The sulfur cycle is one of the most important biogeochemical cycles in these environments, as it is closely linked to the production and consumption of methane (U.S. DOE, 2008). Sulfate reduction, being energetically favored in comparison to fermentative processes and methanogenesis, plays a pivotal role in diminishing gross methane production, consequently curtailing methane emissions into the environment (Capone and Kiene, 1988). The significance of sulfate reduction within coastal wetland soils is well acknowledged, yet the intricacies governing its rates and pathways in these specific environments remain a subject of uncertainty (McCuen et al., 2021). Methanogens are known to be outcompeted by sulfate-reducing bacteria (SRB) for electron donors, which can disrupt microbial activity and lower methane production (An et al., 2023). Saltwater may promote the growth of bacteria that reduce sulfate, which further complicates the biogeochemical processes that take place in wetlands (Jørgensen et al., 2019).

The balance between rates of sea level rise, sulfate intrusion, and wetland accretion will have strong impacts on the capacity to store and sequestering carbon (Yousefi Lalimi et al., 2018; Candry et al., 2023). By the end of the 21st century, ecosystems like eutrophic, shallow, and microtidal estuaries in temperate and high latitudes will be at moderate to high risk of submergence and erosion under future emission scenarios (IPCC , 2022; Yang et al., 2023). There may be conflicting effects among different rates of sea level rise (SLR), with possible increases in net carbon absorption for steadily rising sea levels and net carbon release for faster SLR (IPCC, 2022). The overall response of vegetated coastal ecosystems to rising sea levels is shaped by the diverse interactions among plant growth, sedimentation processes, and inundation(Marani et al., 2006, 2010; Yang et al., 2023). These complex dynamics give rise to contrasting feedback between different scenarios (Gonneea et al., 2019). Biogeochemical studies in wetlands are important for understanding the impact of climate change on the ecosystem services provided by these environments, improving water quality, and mitigating climate change through carbon sequestration (Trettin et al., 2019; Salimi et al., 2021).

In a previous study by Chiapponi et al. (2024), the environmental variables driving CH_4 and CO_2 emissions from temperate coastal wetlands on the Adriatic coast were analyzed and it was shown that salinity and water column level are the major limiting factors of CH_4 emissions in these environments. The present study uses a pioneering multidisciplinary approach to understand the influence of salinity on gas emissions through biogeochemical analysis. Our primary objective is to examine the interplay between microbial communities and sulfur concentrations in hydromorphic soils of three distinct sites, strategically located along a salinity gradient. Specifically, we aim to characterize microbial community composition and structure and to characterize the geochemical composition of the soils harboring the present bacterial communities to investigate the influence of salinity on methanogenic, fermentative, and respiratory pathways that drive the complex processes of organic matter breakdown in temperate coastal wetlands. The biogeochemical results are then discussed with regard to GHG emissions measured in the same areas and reported in Chiapponi et al. (2024). The semiquantitative paper analysis method is applied to assess acid volatile sulfides (AVS) in soils. X-ray fluorescence spectrometry (XRF) was implied to measure elemental composition including total sulfur, while concentrations of total carbon (TC), total hydrogen (TH), total nitrogen (TN), and total organic carbon (TOC) were detected with Elementar Analyzer.

2. Materials and methods

2.1 Study area

The research was conducted in three sites in the province of Ravenna (Italy) (Fig.1), along the Adriatic coast. The San Vitale pine forest and the Punte Alberete marsh are located 3 to 5 km inland of the Northern Adriatic Sea on a dune belt system. The area is characterized by the presence of the Piallassa Baiona, the only brackish intertidal lagoon on the Emilia-Romagna coast. The entire study area is part of the Po River Delta Natural Park and under the European environmental special protection directive (Punte Alberete SCI/SPA IT4070001 and San Vitale pine forest IT4070003 legislation (CEE, 1979, 1992; RER, 2018)).

The area is characterized by a subcontinental temperate climate with about 600 mm of annual rainfall and a monthly mean temperature ranging from 3.6 to 24.3 °C in January and July respectively (ARPAE - Regional Agency for Prevention, Environment and Energy of Emilia-Romagna, weather station of Marina di Ravenna https://simc.arpae.it/dext3r/).
The whole coastal area is highly affected by saltwater intrusion due to both natural and anthropogenic stressors (Antonellini et al., 2019). The unconfined coastal aquifer is primarily based upon beach and dune sandy deposits reaching a depth of 30 m with a central layer of finer sediment (silt) at a depth of 15-16 m (Giambastiani et al., 2007). The only topographical assets above mean sea level are river banks, paleodunes, and current coastal dunes with elevations of 1-3 m a.s.l. Vegetation distribution is impacted by the topographic highs and lows that correlate to various previous coastlines and stages in the evolution of the Po Delta (Amorosi et al., 1999). This low-lying topography causes the coastal phreatic aquifer to be salinized with a sporadic presence of shallow freshwater lenses floating on brackish-salty water and shallow freshwater-saltwater interfaces (Antonellini et al., 2008; Giambastiani et al., 2021). Weather variables, such as temperature, rainfall, and evapotranspiration have a significant impact on the extent of saltwater intrusion in the deep aquifer. Most of the region experiences an increase in groundwater salinity and a drop in water throughout the dry and warm seasons (Giambastiani et al., 2021).
Mechanical drainage is used across the area to regulate floodwater and allow agricultural activities by keeping a steady water table depth of 1.5-2 m below ground level throughout the year (Soboyejo et al., 2021). The intricate network of drain canals and water pumping stations prevents floods but provides a general inland-directed hydraulic gradient, resulting in saltwater intrusion from the salty lagoon and sea (Giambastiani et al., 2021). Salinization of surface and ground waters is particularly substantial around the Piallassa Baiona lagoon, which is directly connected to the Adriatic Sea, along canals and rivers, and in and around those areas

(Antonellini et al., 2008). The water level is also managed in extensive portions of the wetlands, some of which are maintained permanently inundated by a network of ditches and sluices. Compared to natural systems, managed areas where drainage systems regulate water table and flow direction and maintain constant inland hydraulic heads, are more susceptible to climate-change related threats (Giambastiani et al., 2020, 2021). Climate change, SLR and changes in recharge and evapotranspiration patterns will exacerbate the pressure on coastal systems, making the studied areas of Pineta S. Vitale and Punte Alberete particularly vulnerable (Colombani et al., 2016; Giambastiani et al., 2021). The seasonal imbalance in the groundwater budget is exacerbated by the local climate and weather unpredictability (Greggio et al., 2012), with consequences on the biogeochemical cycles of the studied wetlands.

The three selected sites are characterized by a water salinity gradient, ranging from freshwater to slightly brackish to saline waters moving toward the lagoon. Punte Alberete (PA) is the most freshwater site of the area with a mean annual salinity of 0.67 dS m^{-1}; Cerba (CER) is an area characterized by slightly higher salinity, values between 1.4 and 2.2 dS m^{-1}; while Pirottolo (PIR) is characterized by brackish EC values of 6-7.06 dS m^{-1} (Chiapponi et al., 2024).

Based on regional pedological data from the Emilia-Romagna geoportal (https://ambiente.regione. emilia-romagna.it/) and previous research in the area (Buscaroli et al., 2009; Buscaroli and Zannoni, 2010; Ferronato et al., 2016), a succession of soils was observed where topography is the main factor of pedogenesis. The alternation of dunes and lowlands determines a different depth of the water table with respect to the ground level, strongly conditioning the soil moisture regime and the salinity degree. Climatic condition, together with the carbonate sandy substrate and spontaneous vegetation land use generate poorly evolved soil profiles with O/A/C horizon sequence, according to Soil Survey Staff (2022) classification. From the dune crests, where the water table is deepest, to the perennially flooded interdune lowlands, the soil morphosequence is classified as Psamments, Aquents, and Wassents sub-orders according to the Soil Taxonomy (Soil Survey Staff, 2022). In this area, Aquents and Wassents represent hydromorphic and subaqueous soils respectively in a typical coastal transition system (Ferronato et al., 2016). Seasonal variability also affects the soils of this area: spring and autumn rainfall causes salt leaching from soil horizons, a decrease in the water table depth and its salt content dilution; summer weather conditions cause an increase in water table depth and an increase in soil salinity in surface horizons (Buscaroli and Zannoni, 2010, 2017). Changes in the water table level and the total period of saturation have a significant impact on specific soil-forming processes related to the S cycle, $CaCO_3$ accumulation and depletion, and P and salt concentration (Ferronato et al., 2016).

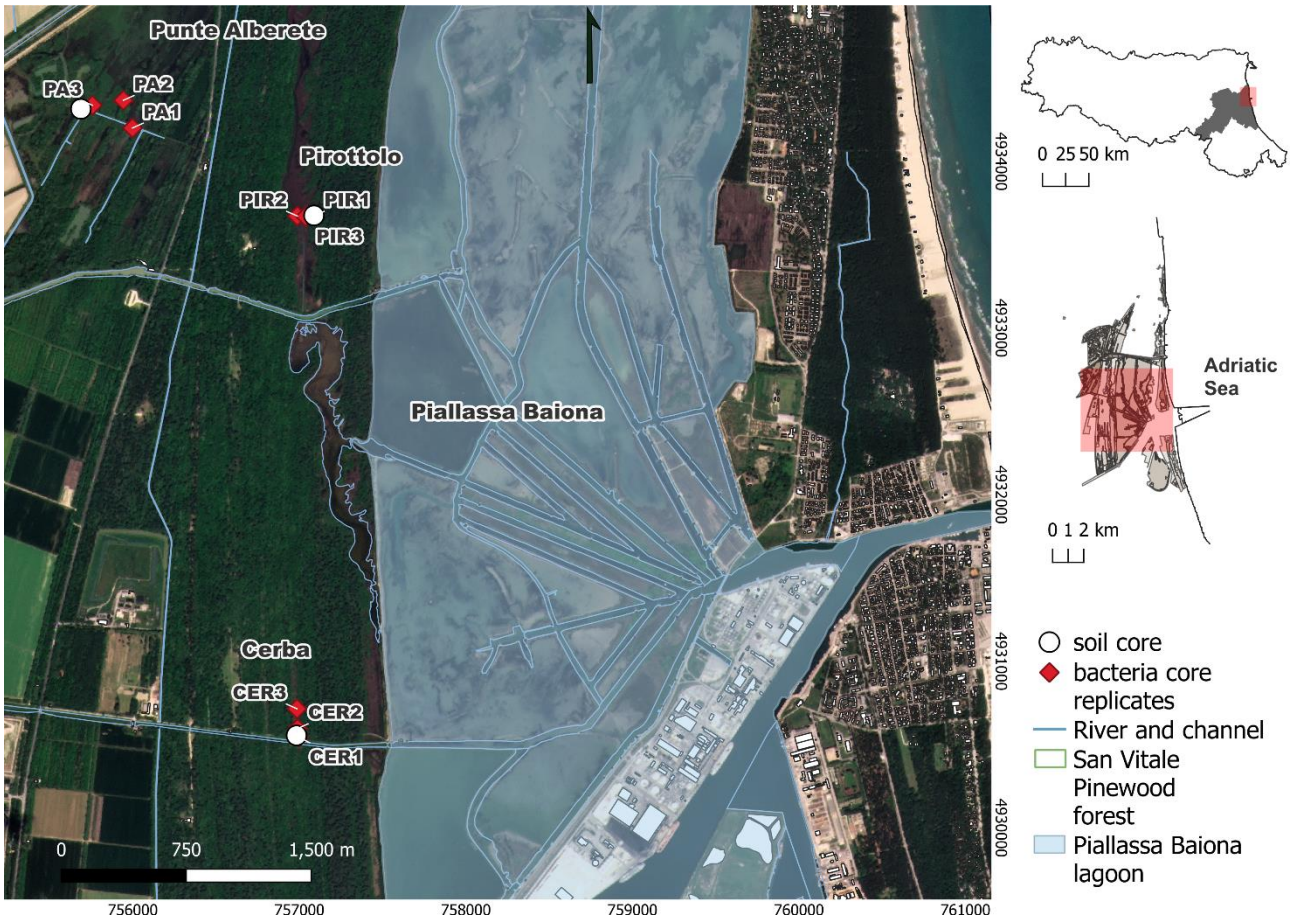

Fig. 1 - Study Area representing the three selected temperate coastal wetlands along with the location of sampled cores for molecular and geochemical analysis (original data elaborated in QGIS 3.26.0; EPSG 32632).

2.2 Sampling (coring)

Cores were taken in four replicates at each location using transparent plexiglass liners. Three cores were used for the molecular analysis, while the fourth core was used to perform the geochemical analysis (Fig.2a). Each core-liner was inserted in soil ensuring that at least 50 cm of soil was retrieved (Fig. 2b). To avoid oxidation, the headspace was filled with water sampled in the same location and immediately sealed with parafilm and tight stopper. To avoid layer mixing, all the tubes have been ensured in vertical position during transport. Corers used for bacterial analysis were previously disinfected with a solution of 20% NaClO to avoid sample contamination. In the laboratory, a section of sediment sample was extruded at 0-20 cm for bacteria analysis (Fig. 2c) from each core and later preserved at -25 °C in sterilized Falcon tubes for DNA extraction. Cores for geochemical analysis were used as a whole and were stored in vertical position at -25 °C until performing any morphological and analytical manipulation.

Fig. 2 – Sediment core sampling design at each location using plexiglass tubes (a and b); core sections at different depths extracted in the laboratory for microbial analysis (B).

2.2 Environmental parameters

Water temperature (°C), pH, Eh (mV) and EC (dS m^{-1}) were measured at each location using probes logged to an EUTECH datalogger. Moreover, to assess the influence of salinity on shaping the bacterial communities, samples of water were collected to analyze sulfate (SO_4^{2-}) and sulfide (S^{2-}) concentrations. At each location, a bottle of water of 500 mL was retrieved without headspace, put in a cooler, and transported to the lab for geochemical analysis, performed on the same day. SO_4^{2-} concentrations have been measured by using a HACH spectrophotometer: 25 mL of sample (pure or diluted) was added into the sample cell, while a blank sample cell was used as reference; Sulfate Ver 4 reagent powder pillow was also added, stirred, and then left for 5 minutes for reaction to take place, and then read to retrieve sulfate concentration (Hach Company, 2019). Similarly, S^{2-} concentration was retrieved by adding 1 mL of Sulfide Reagents 1 and 2 to 25 mL of sample and to deionized water for reference, stirred, and measured after 5 minutes according to the manual instructions (Hach Company, 2014).

2.3 GHG emissions measurements

In the same study area, emissions of CH_4 and CO_2 from open standing waters and soils were measured (Chiapponi et al., 2024). Details about methodology and results are reported in the cited study, which investigated the relationship of abiotic environmental variables with CH_4 and CO_2 emissions in the same temperate coastal wetlands. A summary of the emission rates is provided in Table 2.

2.4 Soil characterization

2.4.1 Pedological characterization

Cores were carefully extruded on a suitable support. Then soil horizon boundaries were identified and marked. For each horizon, thickness, depth, boundaries, matrix Munsell color (moist), texture, structure, fluidity, coats/film, redoximorphic features, peroxide color change, and presence of organic fragments or roots, were described. After the core extrusion, in water-saturated soil samples, pH, electrical conductivity (EC sp), oxidation-reduction potential (ORP), and AVS were measured in each horizon. All other analyses were performed on air-dried soil samples. After drying, EC and pH were measured again for all samples in a 1:2.5 (w:v) soil:distilled water suspension. In the latter also soluble nitrates were determined by Ionic Cromatography. For TOC determination, a carbonates dissolution with 1.5 M HCl was performed before analysis with the elemental analyzer (Thermo Fisher CHNS-O Flash EA 2000) by Dumas flash combustion at 1800 °C, while for TN and TH determination this pretreatment was not necessary (ISO, 1995). To determine

the presence of sulfidic material, an aliquot of each soil horizon was incubated for 16 weeks after which its pH was measured again according to the Soil Survey Staff (2022) methodology.

2.4.2 Sulfides from soils

Acid Volatile Sulfides (AVS) were determined in sampled cores of soils using a semiquantitative method proposed by Pellegrini et al. (2018). The blackening of a paper strip, produced by the precipitation of PbS, was compared with a reference table, previously calibrated. The paper sensor method for S^{2-} is very suitable for field screening and has sensitivity levels comparable to laboratory methods (Pellegrini et al., 2018).

The reference chart was prepared by adding standard S^{2-} solutions ranging from 0.1 to 10 mmol/L following the method suggested by Pellegrini et al. (2018). Paper strips (3x6 cm) were cut from Whatman ® N.1 filter paper and impregnated with 6 drops (approximately 0.3 mL) with 1.5 M $Pb(NO_3)_2$ shortly before use. The impregnated area was roughly 3x4 cm, with the remaining 3 cm dry for pinching the paper strip to a 250 mL polyethylene jar. An aliquot of 10 mL standard solution or fresh soil was placed in the disruptor tube, provided by the extraction kit. The cap was promptly closed after 50 mL of 6M HCl was gently added. The jar was then swirled for about 15 seconds to ensure thorough contact between the soil and the acid and to speed up H_2S volatilization.
The volatilized H_2S combined with the Pb^{2+} on the paper strips to generate PbS, which darkened the paper at a hue proportional to the amount of H_2S developed. The jar was opened after 5 minutes, and the paper strip was removed and immediately compared to the reference colorimetric chart and scanned.

2.4.3 Sulfur characterization

Total sulfur and elemental composition were measured from each soil horizon with X-ray fluorescence (XRF). Each aliquot of dried and milled material was pressed in a thin pallet in a boric acid binder and used to analyze the elemental chemistry with an Axios-Panalytical sequential wavelength dispersive XRF spectrometer with a 4 kW Rh tube and SuperQ 3.0 software. Thermogravimetric analysis was carried out using an Eltra Thermostep thermogravimetric analyzer (Eltra GmbH, Haan, Germany) in an oxidant atmosphere (air, 90 mL min^{-1}) at 10 °C min^{-1} to 600 °C for organic matter determination and then at 25 °C min^{-1} to 950 °C for carbonate determination (Kasozi et al., 2009).

2.5 DNA extraction, 16S rRNA gene amplification and sequencing

From each location and replicate (3 locations, 3 replicates per location), a representative sample of the 0-20 cm core was collected and used for DNA extraction. Total DNA was extracted using the E.Z.N.A.® SOIL DNA KiT (Omega Bio-Tek) inserting 250 mg of the homogenized sample inside the Distruptor Tube provided by the manufacturer. DNA extraction for each sample was performed on the same day together with two negative controls: a tube with only nucleotide-free water and a tube with laboratory aerosol. The latter was prepared by leaving a 2 mL Eppendorf vial open on the laboratory workbench for several hours and later proceeding with the extraction procedure as the biological sample. DNA concentrations were quantified by using the Qubit dsDNA HS As say Kit with a Qubit 2.0 fluorometer (Invitrogen).
The portable DNA sequencer (MinION) from Oxford Nanopore Technologies (ONT) was utilized to characterize the microbial communities (Kerkhof et al., 2017). The MinION is a third-generation platform for direct sequencing of individual strands of DNA translocating nanoscale pores in a semiconductor membrane (Schneider and Dekker, 2012; Wang et al., 2015). Library preparation for the MinION relies on the ligation of adaptor and hairpin to rRNA amplicons. Following the manufacturer's instructions, sequencing libraries were prepared using the 16S Barcoding Kit (SQK-16S024) from Oxford Nanopore Technologies (ONT), Oxford, UK. For each sample, 10 ng of DNA was used for PCR amplification. The PCR procedure consisted of 30 cycles of initial denaturation at 95 °C for 1 minute, denaturation at 95 °C, annealing at 55 °C, and extension at 65 °C, followed by a final extension at 65 °C for 1 minute. Negative PCR controls (PCR reagents without DNA) were amplified at the same time.

Barcoded samples were pooled in equimolar proportions, and about 82 fmol of the pooled sample was loaded into a MinION flow cell (R10.3, FLOMIN111). The flow cell was inserted in the MinION for sequencing and the run, operated by ONT's MinKNOW 4.3.12 software (Oxford Nanopore Technologies, Oxford, UK) lasted for 20 hours and the raw fast5 reads were basecalled and demultiplexed using Guppy v2.3.
Passed reads were analyzed using the EPI2ME pipeline (V5.0.2) using the workflow wf_metagenomics (v2.4.1). The parameter settings of the workflow were: minimum length filter 1350, maximum length filter 1650, minimum read quality 7, batch size 32000, bracken length 10000, and default values in the remaining parameters. The pipeline of this workflow does not process by default reads in the unclassified directory.
Ecological functions of different genus have been assessed using literature references (Tab. 7 Supplementary material), and SILVA (Pruesse et al., 2012) and NCBI (Sayers et al., 2022) databases.

2.6 Statistical Analysis

For all the samples, stacked histograms representing microbial taxa and their relative abundance were drawn using R (version 4.2.2) and "ggplot2" package v.3.4.2 (Wickham, 2016). Only bacteria with more than >0.5% of total relative abundance were considered. Also, all genus presenting a relative abundance <5% have been collapsed into a macro group labelled "Other".
Alpha diversity was calculated for each location (PA, CER, and PIR) on normalized abundance data at genus level as (1) total taxa richness (S), (2) Pielou's Evenness index (J) (Pielou, 1966), and (3) Shannon's index (H'). Pielou's Evenness index estimates the degree of uniformity in the distribution of individuals among different species. The index is maximum when all species are present with the same abundance, instead is low when there is only one abundant, while the Shannon index considers both richness and evenness.
To test the spatial differences in the diversity indexes and on microbial community structure among locations, univariate and multivariate permutational analyses of variance (PERMANOVA) were performed with PERMANOVA+ (Anderson, 2008) using Primer 7 (Clarke and Gorley, 2015). PERMANOVA was based on Euclidean distance matrices for univariate analysis and on Bray-Curtis similarity matrices of square-root transformed data for multivariate. Unconstrained permutation of the raw data with 9999 permutations due to the uneven experimental design (Clarke et al., 2006) were used.
Pattern in the distribution of samples was displayed using a Non-Linear Multi Dimensional Scaling (nMDS) Analysis performed using R software (version 4.2.2)(Oksanen et al., 2022) with the "vegan" package (version 2.6-4). The environmental variables used in the nMDS, have been collected once per location considered the heterogeneity of the environments. Hence, the data regarding geochemical characteristics of soils, such as total lime, AVS, EC, TOC, TN, Fe, S, and ORP have been superimposed.

3. Results

3.1 Geochemical characterization

In Tab. 1, a summary of key geochemical parameters of soil horizons identified in each core are displayed. The morphological features of the soils are reported in Tab. S1 of the Supplementary Materials.

Tab. 1 - Properties of water-saturated soils and air-dried soils for the different horizons. Each row in the table corresponds to a specific horizon within a soil profile (codes according to Soil Survey Staff, 2022), and the columns present parameters retrieved for both water-saturated and air-dried samples. AVS = Acid Volatile Sulfides; TOC = Total Organic Carbon; TN = Total Nitrogen; TOC/TN = Total Organic Carbon to Total Nitrogen ratio; PIR = Pirottolo site; CER = Cerba site; PA = Punte Alberete site. Water reaction on air dryied soil is reported before and after the 16 weeks of incubation ('In pH' and 'Fin pH', respectively).

			Water-saturated soil analysis				Air dry soil analysis					
Profile	**Horizon**	**Depth**	**H_2O reaction**	**EC sp 25 °C**	**Mean ORP**	**S - AVS**	**H_2O reaction**	**EC 1:2.5 25 °C**	**Total lime**	**TOC**	**TN**	**TOC/TN**

		cm	pH	dS m^{-1}	mV	mg kg^{-1}	In pH	Fin pH	dS m^{-1}	g kg^{-1}	g kg^{-1}	g kg^{-1}	
PA	Ase	0 - 4	7.16	0.85	-86	412	7.3	7.75	1.77	191	100.5	6.30	16.0
	Ag	4 - 10	7	0.97	-95	10	7.51	7.71	0.74	144	101.2	5.16	19.6
	Cg1	10 - 17	6.78	1.18	-47	8	7.88	8.01	0.68	231	26.6	2.40	11.1
	Cg2	17 - 32+	7.02	0.96	-68	53	8.11	8.26	0.88	307	13.8	1.46	9.4
CER	Ase	0 - 5	7.37	1.14	-159	1562	7.58	7.74	2.39	283	36.7	3.67	10.0
	Ag	5 - 10	7.27	1.91	-130	174	7.81	7.82	1.52	260	23.5	2.38	9.9
	Cse	10 - 23	7.31	1.44	-223	673	7.96	7.85	1.31	205	11.0	1.21	9.1
	2Cse	23 -35	8.25	1.29	-224	1854	8.56	7.94	0.74	118	2.4	0.24	10.0
PIR	Oi/Ase	0 - 6/7	7.04	5.01	-233	4568	7.26	7.66	7.46	0	119.6	7.14	16.7
	Ase	6/7 - 15	7.43	11.6	-113	1508	7.52	6.96	7.80	0	69.8	4.57	15.3
	A/Cse	15 - 20	7.51	13.8	-77	2461	7.6	7.07	6.03	17	19.5	1.23	15.9
	Cse	20 - 31	7.33	11.8	-198	2168	7.96	6.99	4.27	19	6.5	0.55	11.8
	Cg	31 - 50+	7.34	12.9	-80	658	7.88	7.56	4.79	62	3.4	0.29	11.8

Horizon master: O = organic horizon; A = surface mineral horizon; C = parent material; I = slightly decomposed material; se = presence of sulfides; g = strong gleying.

PA soil profile shows an A/C horizon sequence and consists of 4 horizons, identified as Ase (0 – 4 cm), Ag (4 – 10 cm), Cg1 (10 – 17 cm), and Cg2 (17 - 32+ cm). Texture ranges from silty loam in the upper horizons to silty clay loam in the deeper ones. The color is black (5Y 2.5/1) in the 0-4 cm horizon and grey (5Y 5/1) in the deepest horizon at 17-32+ cm.

The total lime content is the largest at 17-32+ cm with 307 gkg^{-1}. The pH is highest in the superficial layer with 7.16 in the 0-4 cm horizon and decreases to 6.78 at 10-17 cm. This horizon also shows the highest EC value with 1.18 dSm^{-1}, while the lowest is recorded at 0-4 cm with 0.85 dSm^{-1}. Oxidation-reduction potential (ORP) is also the highest in 10-17 cm with -47 mV, while it is the lowest in 0-4 cm and 4-10 cm with value of -86 mV and -95 mV, respectively. The pH after incubation (Fin pH) shows a slight increase in all the horizons. Soluble nitrates show alternating trends, with zero values at 0-4 cm and 10-17 cm depth and a maximum value of 5.32 mg kg^{-1} at the deepest horizon. TOC and TN decrease with depth from 100.5 gkg^{-1} and 6.30 gkg^{-1} at the top horizon, to 13.8 gkg^{-1} and 1.46 gkg^{-1} at the bottom horizon, respectively. S is more concentrated in the 0-4 cm horizon, with a value of 9700 mgkg^{-1}, and gradually decreasing to 2700 mgkg^{-1} in the 17-32+ cm horizon. AVS concentrations are the highest in the 0-4 cm horizon with 412 mgkg^{-1} and the lowest in the middle horizons with 10 mgkg^{-1} and 8 mgkg^{-1} in 4-10 cm and 10-17 cm, respectively. Overall, PA has the highest ORP values and the lowest AVS values compared to the other profiles, suggesting a less reduced and poorer sulfide environment. Based on collected information, this soil profile can be classified as Fluic Frasiwassent, fine-loamy, mixed, calcareous, and mesic (Soil Survey Staff, 2022).

CER soil profile shows an A/C horizon sequence and consists of 4 horizons identified as Ase (0 – 5 cm), Ag (5 – 10 cm), Cse (10 – 23 cm), and 2Cse (23 -35 cm). The soil has a silty loam-silty clay loam texture with sandy loam texture in the 23-35+ cm. The color is greenish black (Gley1 2.5/5GY) in Ase (0 – 5 cm) turning to very dark grey (Gley1 3/N) in 2Cse (23-35+ cm) horizon.

The total lime content is 283 gkg^{-1} in the superficial horizon and decreases with depth to 118 gkg^{-1}. The pH is 7.37 in the 0-5 cm horizon and increases with depth at 23-35+ cm reaching a value of 8.25. EC shows almost constant values along the profile, with the highest value of 1.91 dSm^{-1} at 5-10 cm. ORP decreases along the depth with a starting value of -159 mV in the 0-5 cm horizon, reaching -224 mV at 23-35+ cm of depth. AVS

concentrations are higher at both the most superficial and the deepest horizon with 1562 and 1854 mgkg^{-1} respectively, while it is lower in between. S concentration reflects the same trend with the highest concentrations in the 0-5 cm and 23-35+cm horizon, with values of 2440 mgkg^{-1} and 8910 mgkg^{-1} respectively. On the contrary, Fe concentrations are the lowest at both the most superficial and deepest horizons with 27 and 19.9 gkg^{-1} respectively, while its concentration is higher in between. The two deeper horizons show a slight decrease in pH after the incubation. Soluble nitrates have the highest values in the intermediate horizons (2.3 mgkg^{-1} at 5-10 cm and 1.48 mgkg^{-1} at 10-23 cm), while they tend to zero at both the top and bottom. TOC content is larger in the upper horizons with a starting value of 36.7 gkg^{-1}, gradually diminishing to 2.4 gkg^{-1} at the bottom of the profile. TN shows the same behavior starting with 3.67 gkg^{-1} in the 0-5 cm horizon and decreasing to 0.24 gkg^{-1} in the 23-35 cm horizon. Based on collected information, this soil profile can be classified as Haplic Sulfiwassent, coarse-loamy, mixed, calcareous, and mesic (Soil Survey Staff, 2022).

PIR soil profile shows an O/A/C horizon sequence and consists of 5 horizons identified as Oi/Ase (0 - 6/7 cm), Ase (6/7 – 15 cm), A/Cse (15 – 20 cm), Cse (20 – 31 cm), and Cg (31 - 50+ cm). The soil has a sandy loam texture in the uppermost horizon becoming sandy with depth. The color is black – yellowish (2.5Y 2.5/1) in the 0 – 6/7 cm horizon (Oi/Ase), becoming very dark greenish gray (Gley1 3/10Y) in the 31 - 50 cm (Cg) horizon. The lime content is null in the top horizons and increases to 62 gkg^{-1} in the 31-50+ cm horizon. The soil has a pH of 7.04 which increases to 7.34 in the deeper horizons. EC increases as well, ranging from 5.01 dSm^{-1} in the top to 12.9 dSm^{-1} in the deepest horizon. Similarly, ORP increases from -233 mV in the upper horizon to -80 mV in the bottom horizon. The pH after incubation shows a decrease of 0.5 - 1 unit in the three middle horizons. Soluble nitrates decrease from the top (2.1 mgkg^{-1}) to the intermediate horizons (0.50 mgkg^{-1}) and then increase a little at the bottom (0.91 mgkg^{-1}). Total organic carbon (TOC) is more abundant in the organic-rich layer at the surface with 119.6 gkg^{-1}, decreasing to 3.4 gkg^{-1} in the bottom horizon. Similar behavior can be observed for total nitrogen (TN), with a concentration of 7.14 gkg^{-1} in the superficial horizon, decreasing to 0.29 gkg^{-1} in the deeper horizon. AVS concentrations are higher in the superficial horizon with 4568 mgkg^{-1} in the 0-6/7 cm horizon, decreasing to 658 mgkg^{-1} in the 31-50+ cm horizon. Sulphur (S) content is 2840 mgkg^{-1} at the surface and its concentration remains constant with depth except for the horizon Cse (20-31 cm) where it decreases to 690 mgkg^{-1}. Fe concentration decreases along the profile, starting with a concentration of 34.5 gkg^{-1} at the surface and decreasing to 28.1 gkg^{-1} in the 31-50+ cm horizon. Based on collected information, this soil profile can be classified as Sulfic Psammowassent, mixed, mesic (Soil Survey Staff, 2022).

3.2 GHGs emissions

The GHGs fluxes measured in g m^{-2}day^{-1} across different seasons at the three study sites are presented in Tab. 2 (Chiapponi et al., 2024).

During the Fall-Winter season, the mean CO_2 fluxes varied among the sites. PA showed an average flux of 8.62 ± 13.87 gm^{-2}day^{-1}, CER had 20.34 ± 54.26 g m^{-2}day^{-1}, and PIR exhibited 16.02 ± 7.83 g m^{-2}day^{-1}. For CH_4, PA and PIR recorded mean fluxes of 7.56 ± 33.67 g m^{-2}day^{-1} and 1.99 ± 1.90 g m^{-2}day^{-1}, respectively, while CER presented a substantially higher mean flux of 61.83 ± 250.44 g m^{-2}day^{-1}. In contrast, during the Spring-Summer period, there was a noticeable increase in CO_2 and CH_4 fluxes across all sites. PA, CER, and PIR displayed higher mean CO_2 fluxes of 12.38 ± 17.20 g m^{-2}day^{-1}, 100.62 ± 157.87 g m^{-2}day^{-1}, and 19.37 ± 18.11 g m^{-2}day^{-1}, respectively. Similarly, the mean fluxes of CH_4 rose to 6.04 ± 12.65 g m^{-2}day^{-1}, 254.09 ± 549.93 g m^{-2}day^{-1}, and 15.80 ± 33.89 g m^{-2}day^{-1} for PA, CER, and PIR, respectively. The coefficient of variation percentage indicates higher variability in methane fluxes across both seasons and all sites.

Tab. 2 - Summary of CO_2 and CH_4 fluxes measured in the three studied temperate coastal wetlands by Chiapponi et al. (2024) (Note: n.points = n. point source measured; SD = Standard Deviation; CV(%) = Coefficient of Variation).

Season	GHGs fluxes (g m^{-2}day^{-1})	Punte Alberete (PA)		Cerba (CER)		Bassa del Pirottolo (PIR)	
Fall-Winter		CO_2	CH_4	CO_2	CH_4	CO_2	CH_4

(Oct-Feb)	**n. points**	80	80	121	121	37	37
	mean	8.62	7.56	20.34	61.83	16.02	1.99
	SD	13.87	33.67	54.26	250.44	7.83	1.90
	CV(%)	160.92	445.58	266.77	405.02	48.88	95.70
Spring-Summer (March-Sept)							
	n. points	122	122	177	177	84	84
	mean	12.38	6.04	100.62	254.09	19.37	15.80
	SD	17.20	12.65	157.87	549.93	18.11	33.89
	CV(%)	138.97	209.55	156.90	216.43	93.52	214.52

3.3 Characterization of bacterial communities

MinION sequencing of the 8 core sediment samples yielded 2,639,917 high-quality reads (replicate PA3 was excluded from the analysis due to its low number of reads). On average, 310,254 ± 119,265 reads were obtained for Punte Alberete samples, 365,632 ± 73,054 for Cerba samples, and 264,371 ± 104,047 reads for Pirottolo (Fig.1 in Supplementary Material). Two negative control have been used in the anlysis. Detected contamination was negligible in both negative controls.

3.3.1 Taxonomic composition

The 16S metabarcoding analysis identified 565 families and 3545 genera**.** Sample PA is dominated by genus *Syntrophus* (23.25±0.34%) and *Thiobacillus* (16.68±9.16%), followed by *Haliangium* (8.36±.7.78%), *Clostridium* (7.70±4.91%) as indicated by the prevalence of red/pink colors in Fig. 3.
In the CER location, on the contrary, we observed a prevalence of *Thiobacillus* (19,18±9.77%) and *Sulfuricurvum* (13.76±7.16%)*,* followed by similar mean abundances of *Lysobacter* (9.29±13.66%) and *Desulfuromonas* (9.18±4.66).
In the PIR brackish-water location we observed a different prevalence of taxa compared to the other locations. The most abundant taxa were *Desulfatiglans* (20.04±8.05%), and *Desulfosarcina* (10.69±5.08%), represented by the yellow/green colors. Also, *Algorimarina* (10.17±6.59%), *Thiobacillus* (9.93±10.27%), and *Anaerohalosphaera* (7.73±3.79%) reported moderate high relative abundances.

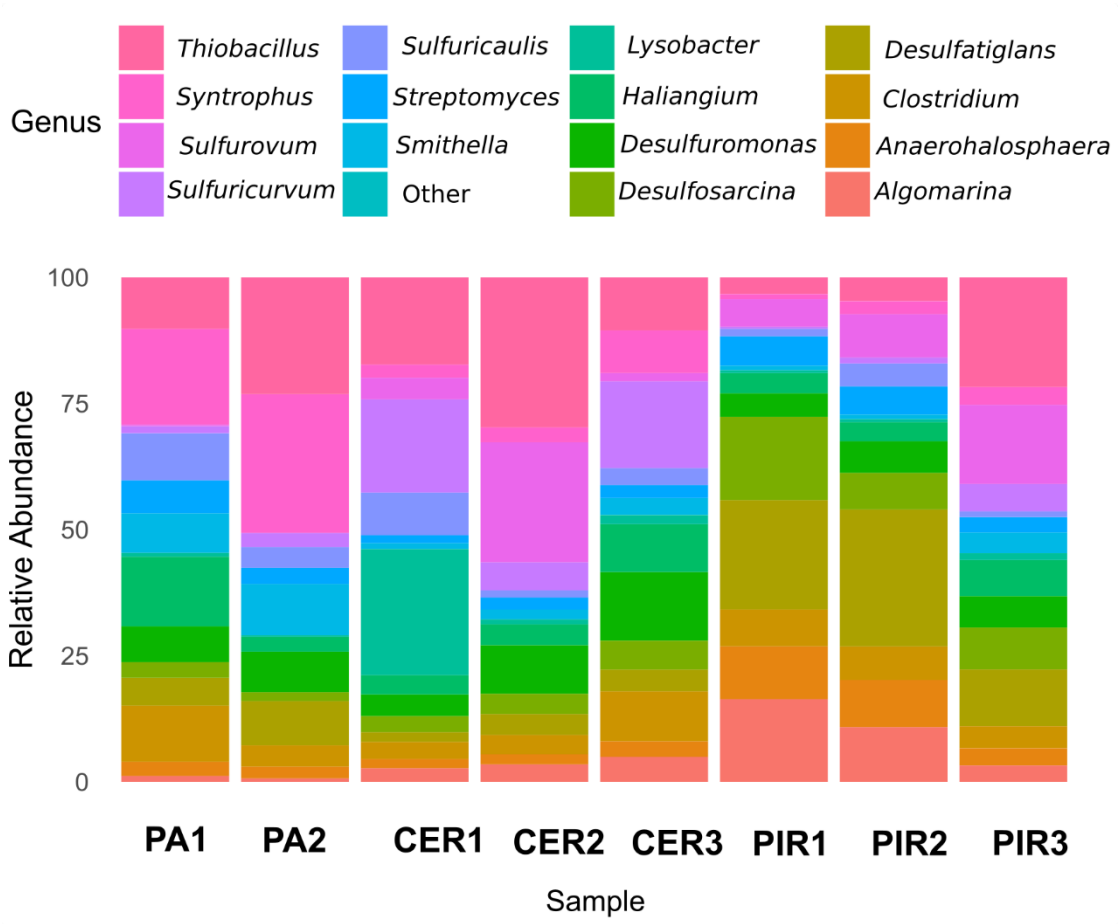

Fig. 3 - Bacterial taxonomic profile (at the genus level) and relative abundance found in each replicate sample. Only taxa representing more than >0.5% of total relative abundance were considered. The class "Other" includes those genera with abundance <5%. Note: Punte Alberete site (PA); Cerba site (CER); Pirottolo (PIR).

3.3.2 Alpha diversity indices

The bacterial communities at the three locations host a comparable Taxa Richness (S) with PA showing an average of 2,690.50±140.50 genus, CER with 2,920.67±56.41 taxa, and PIR with 2,742.67±193.77 taxa (Tab. 2 Supplementary Material)((p>0.05, Tab. 3 Supplementary Material). Pielou's Evenness Index (J) ranged from 0.95±0.01 to 0.96± 0.0007 in PIR and CER, suggesting a high level of evenness in the number and abundance of each genus within these sites)((p>0.05, Tab. 4 Supplementary Material). Shannon's Index (H') values are also very similar among locations)((p>0.05, Tab. 5, Supplementary Material).

3.3.3 Community structural analysis

The bacterial community structures were statistically significant among different locations (P(perm) = 0.004, Tab. 6 Supplementary material) as also evidenced by the nMDS (Fig. 4). In the reduced space of nMDS, PA1 is located in the lower-left quadrant at coordinates MDS1 = -0.24 and MDS2 = -0.27, while PA2 is close at MDS1 = -0.23 and MDS2 = -0.21, demonstrating a resemblance in their lower-left quadrant position. CER1 is in the top portion of the reduced area, with MDS1 = -0.22 and MDS2 = 0.38, indicating dissimilarity to PA1 and PA2. CER2 is in the upper-left quadrant, with MDS1 = -0.04 and MDS2 = 0.09, indicating possible similarities with CER1. CER3, which has MDS1 = -0.15 and MDS2 = 0.07, is also in the upper-left quadrant, showing some dissimilarity to PA1 and PA2. PIR1 is located in the upper-right quadrant, with MDS1 = 0.36 and MDS2 = 0.06, indicating dissimilarity with PA1 and PA2, but probable similarity with CER2 and CER3. PIR2, with MDS1 = 0.42 and MDS2 = -0.09, is in the down half of the reduced area, somewhat to the right of PIR1, showing considerable dissimilarity. PIR3, located in the lower-right quadrant with MDS1 = 0.08 and MDS2 =

-0.03, indicates dissimilarity to CER1, CER2, and CER3. The points distribution on the nMDS plot, are displayed along a salinity range, with freshwater locations on the left quadrant, and brackish locations on the right. In this nMDS analysis, environmental variables such as Total lime, Fe, S, AVS, EC, TN, TOC, and ORP, have been fitted as vectors (Fig. 4). The length and direction of the vectors indicate the direction and strength of the relationship between the variable and the replicates. Upon examination of the plot, we observe that AVS, EC sp 25 °C and EC 1:2.5 25 °C, are aligned along MDS1 influencing replicates from PIR location. On the opposite direction on axis MDS1 is aligned the vector representing Total lime which influences replicates from CER location. S, ORP are aligned on axis MDS2, and their directions indicate an influence on replicates from PA location.

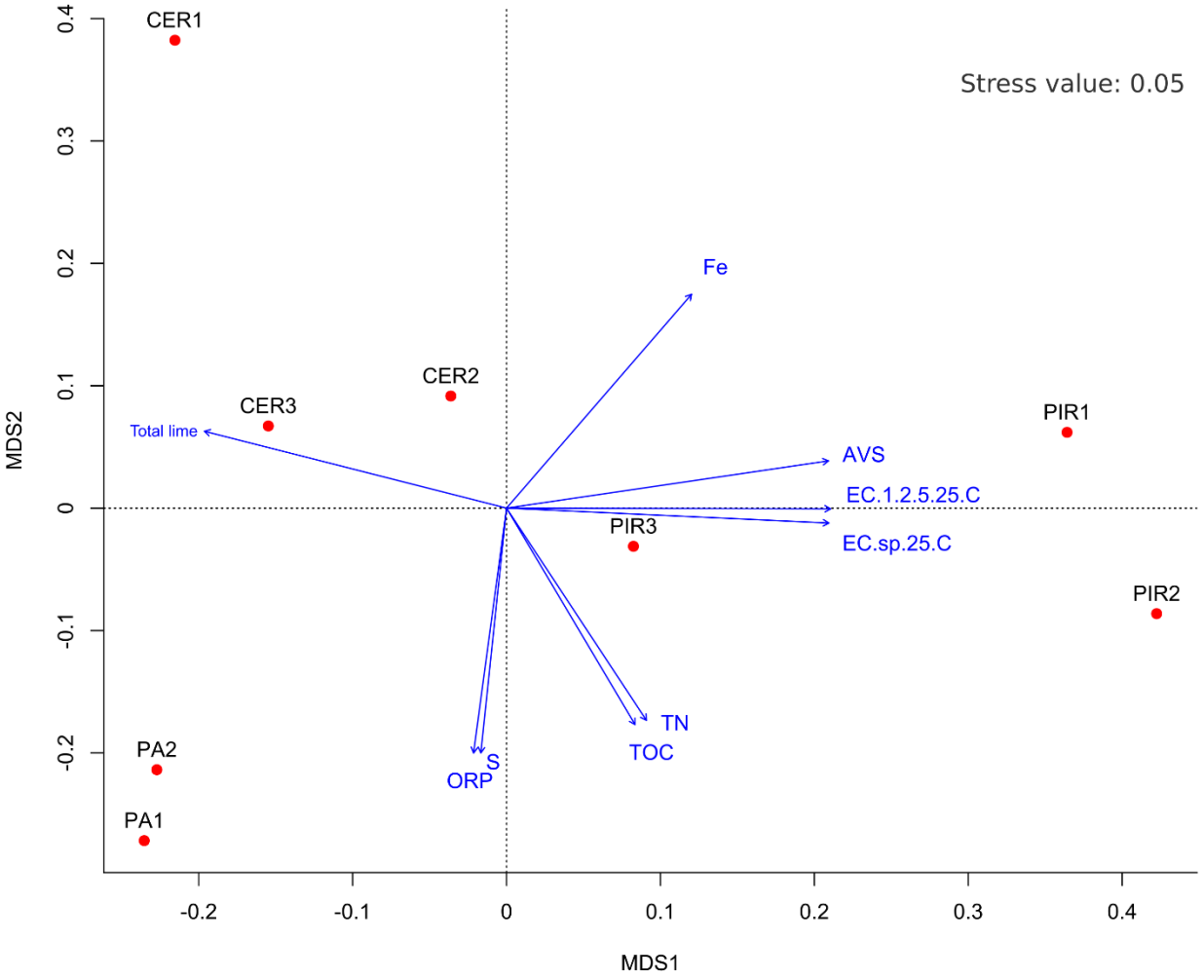

Fig. 4 - Non-Metric Multidimensional Scaling (nMDS) plot of the microbial community structure in the three locations . Punte Alberete site (PA); Cerba site (CER); Pirottolo (PIR).

4. Discussion

Due to their ability to function as carbon sources or sinks, wetlands have a significant impact on the global carbon cycle. Microbially mediated biogeochemical processes, which are further regulated by environmental factors, control the source-sink capacity of wetlands. In this study we investigate the microbial communities at three distinct locations, representing three different temperate coastal wetlands along a salinity gradient: Punte Alberete (PA) is characterized by freshwater ecosystems, Cerba (CER) is another freshwater ecosystem characterized by waters slightly saltier than PA, and Pirottolo (PIR), presenting brackish waters. The

435 significance of salinity as an ecological process driver in tidal fresh-/brackish-water wetlands is particularly
436 important in the study area given the increase of saltwater intrusion, and its exacerbation in the future
437 scenario due to climate change (Giambastiani et al., 2021). The results of this study suggest that salinity and
438 sulfur content lead the major changes in the bacterial community structure along the gradient. The nMDS
439 analysis (Fig. 4) shows that the samples are organized along a salinity gradient from the most freshwater
440 environment, PA, to the most brackish site PIR. PIR exhibits the highest EC compared to CER and PA, explaining
441 the nMDS pattern observed. In PIR location the EC increases from 5.01 dSm^{-1} of the top horizon to 12.9 dSm^{-1}
442 of the bottom horizon. Additionally, Fe concentration is the highest in the PIR site, decreasing from 34.5 gkg^{-1}
443 in the upper horizon to 28.1 gkg^{-1} in the 31-50 cm horizon.

444 Moreover, at the PIR site, the upper horizon contains the highest TOC and TN content, while AVS and S
445 concentrations vary among horizons. The previous study by Chiapponi et al. (2024) performed in the same
446 study site proved that salinity and water column height play a major role in limiting CH_4 and CO_2 emissions in
447 these coastal wetlands. As summarized in Tab. 2, the present study gives a complementary look at how
448 seawater presence allows SRB (Sulfate Reducing Bacteria) to outcompete methanogenic bacteria for carbon
449 substrates (Lovley and Klug, 1986). The presence of sulfate ions favors sulfur-cycling processes in wetland
450 soils to a greater extent at the expense of other redox zone activities, hence decreasing CH_4 emissions
451 (Poffenbarger et al., 2011). Sulphates are abundant in brackish/saline ecosystems, as found in PIR, and act as
452 oxidizing agents in the decomposition of organic matter, reducing methanogenesis and lowering overall
453 emissions (Bridgham et al., 2013; Chiapponi et al., 2024). Because sulfate reduction is more energy-efficient
454 than methanogenesis and fermentative processes, it is critical for lowering gross methane production and, as
455 a result, lowering methane emissions into the environment (Capone and Kiene, 1988).

456 The freshwater location of PA shows a distinct preponderance of *Synthrophus* (23.25±5.99%) (Fig. 4). Its
457 presence is linked to CH_4 production, as syntrophic bacteria engage with methanogenic archaea in
458 cooperative interspecies metabolic interactions, breaking down organic matter into smaller molecules for
459 secondary fermentation, which is the final step in the processes that produce CH_4 (Berrier et al., 2022). Also,
460 *Haliangium* (8.37±7.69%), and *Thiobacillus* (16.68±9.16%) were present (Fig. 4). *Haliangium* is a salt-tolerant
461 myxobacteria found in saline and riparian soils (Fudou et al., 2002) and has a selective predation for
462 methanotrophs and this can explain the almost absence of such taxa in these samples (Kaupper et al., 2022).
463 The presence of *Thiobacillus* suggests the higher potential for sulfur reduction (Bonetti et al., 2021). According
464 to these results, PA has a specialized community, with some genera being essential to the breakdown of
465 organic waste or the cycling of nutrients.
466 In contrast, the structure of the microbial population at the CER site is noticeably different, with the presence
467 of *Lysobacter* (9.29±13.66%%), *Sulfuricurvum* (13.76±7.16%), *Thiobacillus* (19.18± 9.77%), and *Sulfuricaulis*
468 (4.39±3.61%). The existence of these genera—particularly *Thiobacillus*—indicates that the CER ecosystem
469 may be involved in sulfur cycling or other biogeochemical processes. CER stands out with the highest species
470 richness, while the PA site shows the lowest.
471 *Lysobacter* is linked to the presence of Fe(III) in soils (Ko et al., 2009; Luo et al., 2019). Moreover, *Lysobacter*
472 can replace other microorganisms in the system to reduce the competition with sulfate reducing bacteria as
473 electron acceptors (Wang et al., 2021), and can fix and supply nitrogen for other biota and is positive for the
474 reduction of nitrate to nitrite (Iwata et al., 2010). *Sulfuricurvum* and *Thiobacillus* are sulfur oxidizing bacteria
475 (SOBs) that are involved in the oxidation of sulfur compounds and the production of sulfuric acid (Haaijer et
476 al., 2008). These bacteria may be present in soils with high sulfur concentrations (She et al., 2016), like the
477 ones we find both in the topmost (0-5 cm) and the deepest (23-35+ cm) horizons. *Thiobacillus species* may
478 be key players in nitrate-dependent iron sulfide dissolution in freshwater wetlands (Haaijer et al., 2008). This
479 could explain the inverse Pearson correlation between soluble nitrate and AVS in PA and CER soil profiles (-
480 0.99 and -0.45 respectively).

A distinct shift in the microbial community structure is observable at the brackish-water site PIR. . Within PIR, the most prevalent genus is *Desulfatiglans* (20.04±8.05%), along with *Desulfosarcina* (10.69±5.08%), *Algorimarina* (10.17±6.59%), and *Thiobacillus* (9.93±10.27%). The differences in microbial community, compared to PA and CER, imply that the brackish-water location PIR has a distinct microbial community structure, with distinct taxa dominating each sample. In this specific context, *Desulfatiglans* may have a role in sulfur metabolism (Fortin et al., 2000). *Desulfosarcina* is a SRB that can utilize acetate and other fatty acids, oxidizing them completely (Jackson et al., 2014). *Algomarina* spp have a syntrophic butyrate metabolism and are phylogenetically related to SRB from the genera *Desulfonema* and *Desulfosarcina* (McInerney et al., 2008). *Anaerohalosphaera* (7.73±3.79%) is an obligately anaerobic bacteria, moderately halophilic and mesophilic, and can assimilate sulfate (Pradel et al., 2020). Sulfur-cycling process seems also to enhance C mineralization, potentially both reducing CH_4 emissions and enhancing C storage (Candry et al., 2023). *Desulfatiglans* is, ad an example, the most prevalent genus in all samples from PIR, and this is probably linked to its role in sulfur metabolism (Kevorkian et al., 2020). Chiapponi et al. (2024) have in fact clearly shown the low CH_4 fluxes coming from PIR areas but has also enhanced large CO_2 fluxes, comparable to those from freshwater environments, despite the presence of salinity. Similar results were observed in other studies that show how high salinity and CO_2 enhance the presence of SRB (Kim et al., 2020), while decreasing CH_4 emissions (Poffenbarger et al., 2011). However, exceptions are present, as oxidation of reduced sulfur compounds by *Thiobacillus* may release CO_2 as a byproduct (Kleindienst et al., 2014; Jackson et al., 2014). The reduction of sulfate to sulfide and the consequent breakdown of organic materials, which can also lead to the release of CO_2, are also caused by SRB, such as *Desulfatiglans* and *Desulfosarcina* (Kleindienst et al., 2014; Jackson et al., 2014). While SRB competition may prevent the production of CH_4, it may also cause a rise in CO_2 emissions as a consequence, which might counteract the decrease in CH_4 emissions, and the carbon sink capacity of wetlands (Pester, 2012; La et al., 2022). Also, it is known that regular changes in soil redox conditions caused by dry-wet transitions can reduce CH_4 output while increasing N_2O emissions at the same time, offsetting the advantages of CH_4 mitigation (Peyron et al., 2016). The variations in microbial populations responsible for the carbon cycle across sites primarily stem from differences in salinity and sulfate levels. (Fig. 5).

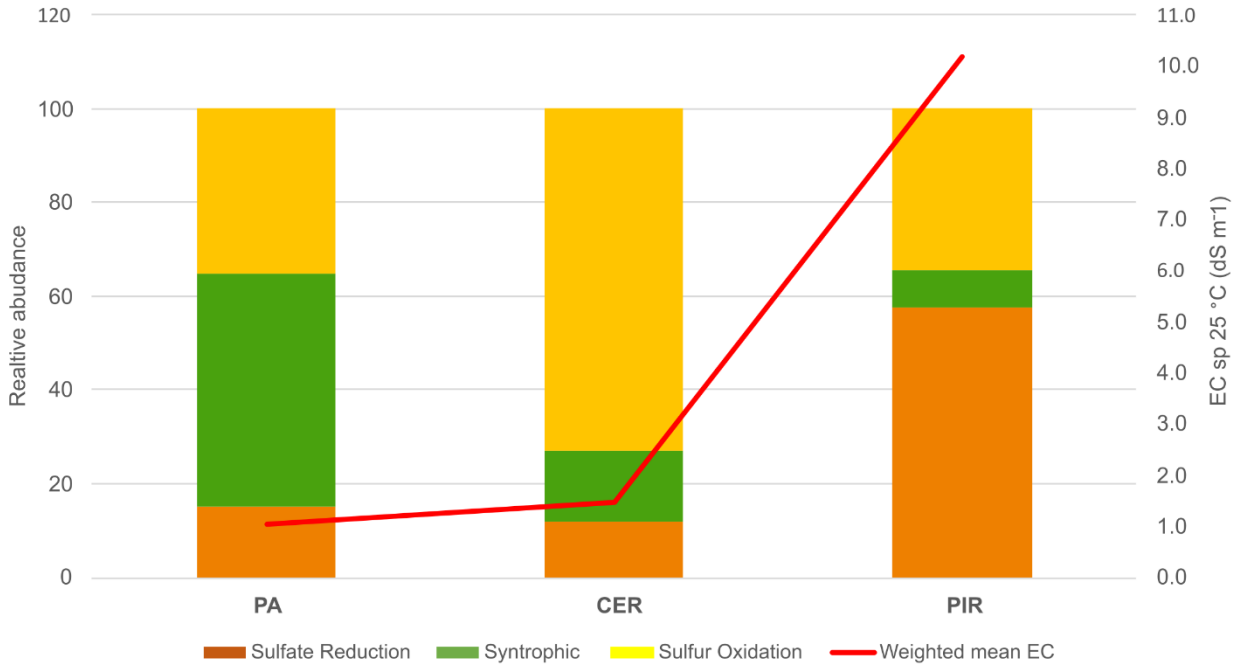

Fig. 5 – Relative genus abundances of the functional groups per location. Functional groups for each genus have been extracted from the cited literature (Tab. 7 - Supplementary material).

Despite having measured CH_4 fluxes in all three sites, no methanogens are found in the sampled soil cores. The absence of methanogens in the soil cores may be due to a variety of factors, including the specific environmental conditions of the studied coastal wetlands (Angel et al., 2012), the limited depth of soil cores, the limited number of replicates for each core because of budget limitations, and the limitations of the experimental design itself. Exposure to oxygen in the soils, among other environmental factors, can decrease methanogen activity (Angel et al., 2012). They are also sensitive to temperature, pH and salt (Angel et al., 2012). Extrusion of soil samples may result in the loss of anoxic conditions existing in the soil. This is because the soil is exposed to oxygen during the extrusion process, which might modify the redox conditions (Fiedler et al., 2007) and lead to the loss of anaerobic microsites where methanogens grow. The depth of the soil cores can affect methanogen identification since deeper soil layers are more likely to retain anoxic conditions than shallow levels. When taking samples from a shallow depth of 20 cm (Angle et al., 2017), the little exchange of oxygen with the water column may not guarantee anoxic conditions, resulting in the lack of methanogens in the samples (Angle et al., 2017).
Further studies at a more detailed level, as an example at each pedological-horizon level and involving more control replicates can be done to investigate the presence and role of methanogens in these complex environments.

5. Conclusion

In this study, we investigated the microbial communities at three distinct temperate coastal wetlands of the Northern Adriatic coast (Italy) along a salinity gradient to assess the interplay between biogeochemical characteristics in submerged soils and GHG emissions. For the first time to our knowledge, a characterization

of the microbial community involved in GHGs production has been conducted in these areas, shedding a light on the C mineralization process occurring in these habitats.

The results suggest that EC and S content lead the major changes in bacterial community structure in different habitats. The clustering analysis reveals three clearly defined clusters of communities that exhibit significant differences from one another: taxa inhabiting freshwater ecosystems, taxa specific to shallow-freshwater habitats, and communities thriving in brackish ecosystems. In freshwater ecosystems like PA and CER, SOB dominate, while in brackish environments like PIR, SRBs are prevalent. The high EC and elevated Fe levels at the brackish-water PIR site drive a shift in bacterial communities towards an abundance of SRB. These findings underscore the role of salinity and sulfur in inhibiting methane CH_4 emissions: the sulfur-rich brackish environment, with its SRB prevalence, shows lower CH_4 emissions compared to freshwater settings.
The study underscores the critical role of characterizing microbial communities in coastal wetlands to unravel their significance in the intricate biogeochemical processes driving carbon cycling. While acknowledging the study's limited scope and the complex nature of wetland systems, it emphasizes a potential trade-off between reduced CH_4 emissions and increased CO_2 emissions with rising salinity levels, as supported by current research (Candry et al., 2023). Although CO_2 is a less potent greenhouse gas than CH_4, higher CO_2 emissions could counterbalance wetlands' carbon sequestration capacity, potentially shifting them from carbon sinks to carbon sources. To craft effective environmental management strategies aimed at mitigating wetlands' global warming potential, it is imperative to consider the diverse greenhouse gas emissions comprehensively (Peyron et al., 2016).
Biogeochemical studies in wetlands play a pivotal role in detecting the intricate interplay between living organisms and environmental factors (Trettin et al., 2019). By delving into the impacts of climate-induced changes like sea level rise and saltwater intrusion on these processes, these studies offer invaluable insights to shape wetland management strategies. This approach not only highlights the long-term health and sustainability of these ecosystems but also contributes to climate change mitigation efforts.

Acknowledgment

This study was performed with the support of the Ravenna municipality (Italy) that granted access to the reserve and the support of the Office for Biodiversity Protection of Punta Marina (Carabinieri Forestali). The authors would like to thank Dr. Francesco Mugnai and Miss. Martina La Torre for the support during the metagenomics analysis and Prof. Enrico Dinelli for performing XRF analysis on samples. This study was carried out within the 490 RETURN Extended Partnership and received funding from the European Union Next-GenerationEU (National Recovery and Resilience Plan – NRRP, Mission 4, Component 2, Investment 1.3 – D.D. 1243 2/8/2022, PE0000005).

We declare to not have any financial or conflicts of interest for any author.

Availability statement

Data used for this research and supplementary materials are freely available ChiapponI, E., Zannoni, D., Giambastiani, B. M. S., Silvestri, S., Buscaroli, A., & Costantini, F. (2024). Dataset and supplementary material for "Investigating Salinity Effect on Temperate Coastal Wetland Soil Microbes and Greenhouse Gas Emissions." [Data set]. Zenodo. https://doi.org/10.5281/zenodo.10479630

References

Amorosi, A., Colalongo, M. L., Pasini, G., and Preti, D.: Sedimentary response to Late Quaternary sea-level changes in the Romagna coastal plain, Sedimentology, 99–121, https://doi.org/10.1046/j.1365-3091.1999.00205.x, 1999.

An, L., Yan, Y.-C., Tian, H.-L., Chi, C.-Q., Nie, Y., and Wu, X.-L.: Roles of sulfate-reducing bacteria in sustaining the diversity and stability of marine bacterial community, Front. Microbiol., 14, 1218828, https://doi.org/10.3389/fmicb.2023.1218828, 2023.

Anderson, M. J.: PERMANOVA+ for PRIMER: guide to software and statistical methods., Primer-E Limited, 2008.

Angel, R., Claus, P., and Conrad, R.: Methanogenic archaea are globally ubiquitous in aerated soils and become active under wet anoxic conditions, ISME J, 6, 847–862, https://doi.org/10.1038/ismej.2011.141, 2012.

Angle, J. C., Morin, T. H., Solden, L. M., Narrowe, A. B., Smith, G. J., Borton, M. A., Rey-Sanchez, C., Daly, R. A., Mirfenderesgi, G., Hoyt, D. W., Riley, W. J., Miller, C. S., Bohrer, G., and Wrighton, K. C.: Methanogenesis in oxygenated soils is a substantial fraction of wetland methane emissions, Nat Commun, 8, 1567, https://doi.org/10.1038/s41467-017-01753-4, 2017.

Antonellini, M., Mollema, P., Giambastiani, B., Bishop, K., Caruso, L., Minchio, A., Pellegrini, L., Sabia, M., Ulazzi, E., and Gabbianelli, G.: Salt water intrusion in the coastal aquifer of the southern Po Plain, Italy, Hydrogeol J, 16, 1541–1556, https://doi.org/10.1007/s10040-008-0319-9, 2008.

Antonellini, M., Giambastiani, B. M. S., Greggio, N., Bonzi, L., Calabrese, L., Luciani, P., Perini, L., and Severi, P.: Processes governing natural land subsidence in the shallow coastal aquifer of the Ravenna coast, Italy, CATENA, 172, 76–86, https://doi.org/10.1016/j.catena.2018.08.019, 2019.

Berrier, D. J., Neubauer, S. C., and Franklin, R. B.: Cooperative microbial interactions mediate community biogeochemical responses to saltwater intrusion in wetland soils, FEMS Microbiology Ecology, 98, fiac019, https://doi.org/10.1093/femsec/fiac019, 2022.

Bonetti, G., Trevathan-Tackett, S. M., Carnell, P. E., Treby, S., and Macreadie, P. I.: Local vegetation and hydroperiod influence spatial and temporal patterns of carbon and microbe response to wetland rehabilitation, Applied Soil Ecology, 163, 103917, https://doi.org/10.1016/j.apsoil.2021.103917, 2021.

Bridgham, S. D., Cadillo-Quiroz, H., Keller, J. K., and Zhuang, Q.: Methane emissions from wetlands: biogeochemical, microbial, and modeling perspectives from local to global scales, Glob Change Biol, 19, 1325–1346, https://doi.org/10.1111/gcb.12131, 2013.

Buscaroli, A. and Zannoni, D.: Influence of ground water on soil salinity in the San Vitale Pinewood (Ravenna - Italy), Vol. LIV-N. 5, 2010.

Buscaroli, A. and Zannoni, D.: Soluble ions dynamics in Mediterranean coastal pinewood forest soils interested by saline groundwater, CATENA, 157, 112–129, https://doi.org/10.1016/j.catena.2017.05.014, 2017.

Buscaroli, A., Gherardi, M., Vianello, G., Vittori Antisari, L., and Zannoni, D.: Soil survey and classification in a complex territorial system: Ravenna (italy), EQA - International Journal of Environmental Quality, Vol. 2, 15–28, https://doi.org/10.6092/ISSN.2281-4485/3815, 2009.

Candry, P., Abrahamson, B., Stahl, D. A., and Winkler, M. H.: Microbially mediated climate feedbacks from wetland ecosystems, Global Change Biology, 29, 5169–5183, https://doi.org/10.1111/gcb.16850, 2023.

Capaccioni, B., Tassi, F., Cremonini, S., Sciarra, A., and Vaselli, O.: Ground heating and methane oxidation processes at shallow depth in Terre Calde di Medolla (Italy): Observations and conceptual

615 model: SOIL HEATING DUE TO METHANE OXIDATION, J. Geophys. Res. Solid Earth, 120,
616 3048–3064, https://doi.org/10.1002/2014JB011635, 2015.

617 Capone, D. G. and Kiene, R. P.: Comparison of microbial dynamics in marine and freshwater
618 sediments: Contrasts in anaerobic carbon catabolism1: Microbial dynamics in sediments, Limnol.
619 Oceanogr., 33, 725–749, https://doi.org/10.4319/lo.1988.33.4part2.0725, 1988.

620 Cardellini, C., Chiodini, G., Frondini, F., Granieri, D., Lewicki, J., and Peruzzi, L.: Accumulation
621 chamber measurements of methane fluxes: application to volcanic-geothermal areas and landfills,
622 Applied Geochemistry, 18, 45–54, https://doi.org/10.1016/S0883-2927(02)00091-4, 2003.

623 Chiapponi, E., Silvestri, S., Zannoni, D., Antonellini, M., and Giambastiani, B. M. S.: Driving and
624 limiting factors of CH_4 and CO_2 emissions from coastal brackish-water wetlands in temperate
625 regions, Biogeosciences, 21, 73–91, https://doi.org/10.5194/bg-21-73-2024, 2024.

626 Clarke, K. R. and Gorley, R. N.: Getting started with PRIMER v7, vol. PRIMER-E, lymouth:
627 Plymouth Marine Laboratory, 2015.

628 Clarke, K. R., Somerfield, P. J., and Chapman, M. G.: On resemblance measures for ecological
629 studies, including taxonomic dissimilarities and a zero-adjusted Bray–Curtis coefficient for denuded
630 assemblages, Journal of Experimental Marine Biology and Ecology, 330, 55–80,
631 https://doi.org/10.1016/j.jembe.2005.12.017, 2006.

632 D. Fortin, R. Goulet, M. Roy: Seasonal Cycling of Fe and S in a Constructed Wetland: The Role of
633 Sulfate-Reducing Bacteria, Geomicrobiology Journal, 17, 221–235,
634 https://doi.org/10.1080/01490450050121189, 2000.

635 Dang, C., Morrissey, E. M., Neubauer, S. C., and Franklin, R. B.: Novel microbial community
636 composition and carbon biogeochemistry emerge over time following saltwater intrusion in
637 wetlands, Global Change Biology, 25, 549–561, https://doi.org/10.1111/gcb.14486, 2019.

638 Duarte, C. M., Losada, I. J., Hendriks, I. E., Mazarrasa, I., and Marbà, N.: The role of coastal plant
639 communities for climate change mitigation and adaptation, Nature Clim Change, 3, 961–968,
640 https://doi.org/10.1038/nclimate1970, 2013.

641 EEC - Council of the European Union: Council Directive 79/409/EEC of 2 April 1979 on the
642 conservation of wild birds.pdf, OJ L 103, 1–18, 1979.

643 EEC - Council of the European Union: Council Directive 92/43/EEC of 21 May 1992 on the
644 conservation of natural habitats and of wild fauna and flora, Official Journal L 206, 92/43/EEC, P.
645 7-50, 1992.

646 Ferronato, C., Falsone, G., Natale, M., Zannoni, D., Buscaroli, A., Vianello, G., and Vittori
647 Antisari, L.: Chemical and pedological features of subaqueous and hydromorphic soils along a
648 hydrosequence within a coastal system (San Vitale Park, Northern Italy), Geoderma, 265, 141–151,
649 https://doi.org/10.1016/j.geoderma.2015.11.018, 2016.

650 Fiedler, S., Vepraskas, M. J., and Richardson, J. L.: Soil Redox Potential: Importance, Field
651 Measurements, and Observations, in: Advances in Agronomy, vol. 94, Elsevier, 1–54,
652 https://doi.org/10.1016/S0065-2113(06)94001-2, 2007.

653 Fudou, R., Jojima, Y., Iizuka, T., and Yamanaka, S.: Haliangium ochraceum gen. nov., sp. nov. and
654 Haliangium tepidum sp. nov.: Novel moderately halophilic myxobacteria isolated from coastal

655 saline environments., J. Gen. Appl. Microbiol., 48, 109–115, https://doi.org/10.2323/jgam.48.109,
656 2002.

657 Giambastiani, B. M. S., Antonellini, M., Oude Essink, G. H. P., and Stuurman, R. J.: Saltwater
658 intrusion in the unconfined coastal aquifer of Ravenna (Italy): A numerical model, Journal of
659 Hydrology, 340, 91–104, https://doi.org/10.1016/j.jhydrol.2007.04.001, 2007.

660 Giambastiani, B. M. S., Kidanemariam, A., Dagnew, A., and Antonellini, M.: Evolution of Salinity
661 and Water Table Level of the Phreatic Coastal Aquifer of the Emilia Romagna Region (Italy),
662 Water, 13, 372, https://doi.org/10.3390/w13030372, 2021.

663 Gonneea, M. E., Maio, C. V., Kroeger, K. D., Hawkes, A. D., Mora, J., Sullivan, R., Madsen, S.,
664 Buzard, R. M., Cahill, N., and Donnelly, J. P.: Salt marsh ecosystem restructuring enhances
665 elevation resilience and carbon storage during accelerating relative sea-level rise, Estuarine, Coastal
666 and Shelf Science, 217, 56–68, https://doi.org/10.1016/j.ecss.2018.11.003, 2019.

667 Haaijer, S. C. M., Harhangi, H. R., Meijerink, B. B., Strous, M., Pol, A., Smolders, A. J. P.,
668 Verwegen, K., Jetten, M. S. M., and Op Den Camp, H. J. M.: Bacteria associated with iron seeps in
669 a sulfur-rich, neutral pH, freshwater ecosystem, ISME J, 2, 1231–1242,
670 https://doi.org/10.1038/ismej.2008.75, 2008.

671 Hach Company: Sulfide, Methylene Blue Method, Method 10254, 2014.

672 Hach Company: Sulfate, SulfaVer 4 Method (70 mg/L), 2019.

673 Hopkinson, C. S., Cai, W.-J., and Hu, X.: Carbon sequestration in wetland dominated coastal
674 systems—a global sink of rapidly diminishing magnitude, Current Opinion in Environmental
675 Sustainability, 4, 186–194, https://doi.org/10.1016/j.cosust.2012.03.005, 2012.

676 ISO - International Standard Organization, S.: ISO 10694:1995, Soil quality - Determination of
677 organic and total carbon after dry combustion (elementary analysis), Technical Committee ISO/TC
678 190, 1995.

679 IPCC - Intergovernmental Panel On Climate Change (Ipcc): The Ocean and Cryosphere in a
680 Changing Climate: Special Report of the Intergovernmental Panel on Climate Change, 1st ed.,
681 Cambridge University Press, https://doi.org/10.1017/9781009157964, 2022.

682 Iwata, K., Azlan, A., Yamakawa, H., and Omori, T.: Ammonia accumulation in culture broth by the
683 novel nitrogen-fixing bacterium, Lysobacter sp. E4, Journal of Bioscience and Bioengineering, 110,
684 415–418, https://doi.org/10.1016/j.jbiosc.2010.05.006, 2010.

685 Jackson, K. L., Whitcraft, C. R., and Dillon, J. G.: Diversity of Desulfobacteriaceae and Overall
686 Activity of Sulfate-Reducing Microorganisms in and Around a Salt pan in a Southern California
687 Coastal Wetland, Wetlands, 34, 969–977, https://doi.org/10.1007/s13157-014-0560-z, 2014.

688 Jørgensen, B. B., Findlay, A. J., and Pellerin, A.: The Biogeochemical Sulfur Cycle of Marine
689 Sediments, Front. Microbiol., 10, 849, https://doi.org/10.3389/fmicb.2019.00849, 2019.

690 Kasozi, G. N., Nkedi-Kizza, P., and Harris, W. G.: Varied Carbon Content of Organic Matter in
691 Histosols, Spodosols, and Carbonatic Soils, Soil Sci. Soc. Am. J., 73, 1313–1318,
692 https://doi.org/10.2136/sssaj2008.0070, 2009.

693 Kaupper, T., Mendes, L. W., Poehlein, A., Frohloff, D., Rohrbach, S., Horn, M. A., and Ho, A.: The
694 methane-driven interaction network in terrestrial methane hotspots, Environmental Microbiome, 17,
695 15, https://doi.org/10.1186/s40793-022-00409-1, 2022.

696 Kerkhof, L. J., Dillon, K. P., Häggblom, M. M., and McGuinness, L. R.: Profiling bacterial
697 communities by MinION sequencing of ribosomal operons, Microbiome, 5, 116,
698 https://doi.org/10.1186/s40168-017-0336-9, 2017.

699 Kevorkian, R., Callahan, S., Winstead, R., and Lloyd, K. G.: ANME-1 archaea drive methane
700 accumulation and removal in estuarine sediments, Microbiology,
701 https://doi.org/10.1101/2020.02.24.963215, 2020.

702 Kim, S.-Y., Freeman, C., Lukac, M., Lee, S.-H., Kim, S. D., and Kang, H.: Elevated CO2 and high
703 salinity enhance the abundance of sulfate reducers in a salt marsh ecosystem, Applied Soil Ecology,
704 147, 103386, https://doi.org/10.1016/j.apsoil.2019.103386, 2020.

705 Kleindienst, S., Herbst, F.-A., Stagars, M., Von Netzer, F., Von Bergen, M., Seifert, J., Peplies, J.,
706 Amann, R., Musat, F., Lueders, T., and Knittel, K.: Diverse sulfate-reducing bacteria of the
707 Desulfosarcina/Desulfococcus clade are the key alkane degraders at marine seeps, ISME J, 8, 2029–
708 2044, https://doi.org/10.1038/ismej.2014.51, 2014.

709 Ko, H.-S., Jin, R.-D., Krishnan, H. B., Lee, S.-B., and Kim, K.-Y.: Biocontrol Ability of Lysobacter
710 antibioticus HS124 Against Phytophthora Blight Is Mediated by the Production of 4-
711 Hydroxyphenylacetic Acid and Several Lytic Enzymes, Curr Microbiol, 59, 608–615,
712 https://doi.org/10.1007/s00284-009-9481-0, 2009.

713 La, W., Han, X., Liu, C.-Q., Ding, H., Liu, M., Sun, F., Li, S., and Lang, Y.: Sulfate concentrations
714 affect sulfate reduction pathways and methane consumption in coastal wetlands, Water Research,
715 217, 118441, https://doi.org/10.1016/j.watres.2022.118441, 2022.

716 Liang, S., Li, H., Wu, H., Yan, B., and Song, A.: Microorganisms in coastal wetland sediments: a
717 review on microbial community structure, functional gene, and environmental potential, Front.
718 Microbiol., 14, 1163896, https://doi.org/10.3389/fmicb.2023.1163896, 2023.

719 Luo, M., Huang, J.-F., Zhu, W.-F., and Tong, C.: Impacts of increasing salinity and inundation on
720 rates and pathways of organic carbon mineralization in tidal wetlands: a review, Hydrobiologia,
721 827, 31–49, https://doi.org/10.1007/s10750-017-3416-8, 2019.

722 Marani, M., Zillio, T., Belluco, E., Silvestri, S., and Maritan, A.: Non-Neutral Vegetation
723 Dynamics, PLoS ONE, 1, e78, https://doi.org/10.1371/journal.pone.0000078, 2006.

724 Marani, M., D'Alpaos, A., Lanzoni, S., Carniello, L., and Rinaldo, A.: The importance of being
725 coupled: Stable states and catastrophic shifts in tidal biomorphodynamics, J. Geophys. Res., 115,
726 2009JF001600, https://doi.org/10.1029/2009JF001600, 2010.

727 McCuen, M. M., Pitesky, M. E., Buler, J. J., Acosta, S., Wilcox, A. H., Bond, R. F., and Díaz-
728 Muñoz, S. L.: A comparison of amplification methods to detect Avian Influenza viruses in
729 California wetlands targeted via remote sensing of waterfowl, Transbound Emerg Dis, 68, 98–109,
730 https://doi.org/10.1111/tbed.13612, 2021.

731 McInerney, M. J., Struchtemeyer, C. G., Sieber, J., Mouttaki, H., Stams, A. J. M., Schink, B.,
732 Rohlin, L., and Gunsalus, R. P.: *Physiology, Ecology, Phylogeny, and Genomics of Microorganisms*

733 *Capable of Syntrophic Metabolism*, Annals of the New York Academy of Sciences, 1125, 58–72,
734 https://doi.org/10.1196/annals.1419.005, 2008.

735 Mitsch, W. J., Bernal, B., Nahlik, A. M., Mander, Ü., Zhang, L., Anderson, C. J., Jørgensen, S. E.,
736 and Brix, H.: Wetlands, carbon, and climate change, Landscape Ecol, 28, 583–597,
737 https://doi.org/10.1007/s10980-012-9758-8, 2013.

738 Morrissey, E. M., Gillespie, J. L., Morina, J. C., and Franklin, R. B.: Salinity affects microbial
739 activity and soil organic matter content in tidal wetlands, Global Change Biology, 20, 1351–1362,
740 https://doi.org/10.1111/gcb.12431, 2014.

741 Oksanen, J., Simpson, G., Blanchet, F. G., Kindt, R., Legendre, P., R. Minchin, P., O'Hara, R. B.,
742 Solymos, P., Stevens, M. H. H., Szoecs, E., Wagner, H., Barbour, M., Bedward, M., Bolker, B.,
743 Borcard, D., Carvalho, G., Chirico, M., DE Caceres, M., Durand, S., Antoniazi Evangelista, H. B.,
744 FitzJohn, R., Friendly, M., Furneaux, B., Hannigan, G., Hill, M. O., Lahti, L., McGlinn, D.,
745 Ouellette, M.-H., Ribeiro Cunha, E., Smith, T., Adrian, S., Ter Braak, C. J. F., and Weedon, J.:
746 Community Ecology Package, 2022.

747 Pellegrini, E., Contin, M., Vittori Antisari, L., Vianello, G., Ferronato, C., and De Nobili, M.: A
748 new paper sensor method for field analysis of acid volatile sulfides in soils: Paper sensor method for
749 field analysis of acid volatile sulfides, Environ Toxicol Chem, 37, 3025–3031,
750 https://doi.org/10.1002/etc.4279, 2018.

751 Pester, M.: Sulfate-reducing microorganisms in wetlands – fameless actors in carbon cycling and
752 climate change, Front. Microbio., 3, https://doi.org/10.3389/fmicb.2012.00072, 2012.

753 Peyron, M., Bertora, C., Pelissetti, S., Said-Pullicino, D., Celi, L., Miniotti, E., Romani, M., and
754 Sacco, D.: Greenhouse gas emissions as affected by different water management practices in
755 temperate rice paddies, Agriculture, Ecosystems & Environment, 232, 17–28,
756 https://doi.org/10.1016/j.agee.2016.07.021, 2016.

757 Poffenbarger, H. J., Needelman, B. A., and Megonigal, J. P.: Salinity Influence on Methane
758 Emissions from Tidal Marshes, Wetlands, 31, 831–842, https://doi.org/10.1007/s13157-011-0197-
759 0, 2011.

760 Pradel, N., Fardeau, M.-L., Tindall, B. J., and Spring, S.: Anaerohalosphaera lusitana gen. nov., sp.
761 nov., and Limihaloglobus sulfuriphilus gen. nov., sp. nov., isolated from solar saltern sediments,
762 and proposal of Anaerohalosphaeraceae fam. nov. within the order Sedimentisphaerales,
763 International Journal of Systematic and Evolutionary Microbiology, 70, 1321–1330,
764 https://doi.org/10.1099/ijsem.0.003919, 2020.

765 Pruesse, E., Peplies, J., and Glöckner, F. O.: SINA: Accurate high-throughput multiple sequence
766 alignment of ribosomal RNA genes, Bioinformatics, 28, 1823–1829,
767 https://doi.org/10.1093/bioinformatics/bts252, 2012.

768 RER - Regione Emilia Romagna: MISURE SPECIFICHE DI CONSERVAZIONE DEL SIC-ZPS
769 IT4070003 "PINETA DI SAN VITALE, BASSA DEL PIROTTOLO," 2018.

770 Salimi, S., Almuktar, S. A. A. A. N., and Scholz, M.: Impact of climate change on wetland
771 ecosystems: A critical review of experimental wetlands, Journal of Environmental Management,
772 286, 112160, https://doi.org/10.1016/j.jenvman.2021.112160, 2021.

773 Sayers, E. W., Bolton, E. E., Brister, J. R., Canese, K., Chan, J., Comeau, D. C., Connor, R., Funk,
774 K., Kelly, C., Kim, S., Madej, T., Marchler-Bauer, A., Lanczycki, C., Lathrop, S., Lu, Z., Thibaud-
775 Nissen, F., Murphy, T., Phan, L., Skripchenko, Y., Tse, T., Wang, J., Williams, R., Trawick, B. W.,
776 Pruitt, K. D., and Sherry, S. T.: Database resources of the national center for biotechnology
777 information, Nucleic Acids Research, 50, D20–D26, https://doi.org/10.1093/nar/gkab1112, 2022.

778 Schneider, G. F. and Dekker, C.: DNA sequencing with nanopores, Nat Biotechnol, 30, 326–328,
779 https://doi.org/10.1038/nbt.2181, 2012.

780 Schoeneberger, P. J., Wysocki, D. A., Benham, E. C., and Soil. Survey Staff: Field Book for
781 Describing and Sampling Soils; Version 3.0, , National Soil Survey Center, Lincoln, NE, 2012.

782 She, C. X., Zhang, Z. C., Cadillo-Quiroz, H., and Tong, C.: Factors regulating community
783 composition of methanogens and sulfate-reducing bacteria in brackish marsh sediments in the Min
784 River estuary, southeastern China, Estuarine, Coastal and Shelf Science, 181, 27–38,
785 https://doi.org/10.1016/j.ecss.2016.08.003, 2016.

786 SSS - Soil Survey Staff and United States Department of Agriculture Natural Resources
787 Conservation Service: Keys to Soil Taxonomy, 13th Edition, 2022.

788 Trettin, C. C., Jurgensen, M. F., and Dai, Z.: Effects of climate change on forested wetland soils, in:
789 Developments in Soil Science, vol. 36, Elsevier, 171–188, https://doi.org/10.1016/B978-0-444-
790 63998-1.00009-4, 2019.

791 U.S. DOE: Carbon Cycling and Biosequestration Integrating Biology and Climate Through Systems
792 Science, U.S. Department of Energy Office of Science Office of Biological and Environmental
793 Research, 2008.

794 Wang, Q., Zhou, G., Qin, Y., Wang, R., Li, H., Xu, F., Du, Y., Zhao, C., Zhang, H., and Kong, Q.:
795 Sulfate removal performance and co-occurrence patterns of microbial community in constructed
796 wetlands treating saline wastewater, Journal of Water Process Engineering, 43, 102266,
797 https://doi.org/10.1016/j.jwpe.2021.102266, 2021.

798 Wang, Y., Yang, Q., and Wang, Z.: The evolution of nanopore sequencing, Front. Genet., 5,
799 https://doi.org/10.3389/fgene.2014.00449, 2015.

800 White, E. and Kaplan, D.: Restore or retreat? saltwater intrusion and water management in coastal
801 wetlands, Ecosyst Health Sustain, 3, e01258, https://doi.org/10.1002/ehs2.1258, 2017.

802 Yang, Z., Tognin, D., Finotello, A., Belluco, E., Puppin, A., Silvestri, S., Marani, M., and
803 D'Alpaos, A.: Long-Term Monitoring of Coupled Vegetation and Elevation Changes in Response
804 to Sea Level Rise in a Microtidal Salt Marsh, JGR Biogeosciences, 128, e2023JG007405,
805 https://doi.org/10.1029/2023JG007405, 2023.

806 Yousefi Lalimi, F., Silvestri, S., D'Alpaos, A., Roner, M., and Marani, M.: The Spatial Variability
807 of Organic Matter and Decomposition Processes at the Marsh Scale, JGR Biogeosciences, 123,
808 3713–3727, https://doi.org/10.1029/2017JG004211, 2018.

809

JGR - Biogeosciences

Supporting Information for

Investigating Salinity Effect on Temperate Coastal Wetland Soil Microbes and Greenhouse Gas Emissions.

Emilia Chiapponi[1], Denis Zannoni[1], Beatrice Maria Sole Giambastiani[1], Sonia Silvestri[1], Alessandro Buscaroli[1], Federica Costantini[1]

[1]Biological, Geological and Environmental Sciences Department, University of Bologna, Ravenna Campus, Italy

**Corresponding Author*: Emilia Chiapponi (emilia.chiapponi2@unibo.it)

Contents of this file

Tables S1 to S7

Introduction

In this supporting information tables about morphological features of soils profiles analyzed for this research can be found. Also, results for diversity index of the microbial community in the three different studied locations are reported, along ANOVA results. This section also reports the bibliography used to identify ecological function of the most abundant genus in the soil profiles analyzed.

Original data and statistical analysis processes are freely available at at Chiapponi, E., Zannoni, D., Giambastiani, B. M. S., Silvestri, S., Buscaroli, A., & Costantini, F. (2024). Dataset and supplementary material for "Investigating Salinity Effect on Temperate Coastal Wetland Soil Microbes and Greenhouse Gas Emissions." [Data set]. Zenodo. https://doi.org/10.5281/zenodo.10479630

Tab. S 1 Morphological features of soil profiles

Profile	Horizon		Boundary (D/T)	Matrix Munsell Color (Wet)	Field texture class	Structure (T/G/S)	Fluidity class	Mottles/RMFs (K/Q/S/Sh)	Mottles/RMFs Munsell Color (WET)	Peroxide Color Change (Y/N)	Organic frag/Roots (Q/S)	Odor (K/I)
	Depth (cm)	Master										
PIR	0 - 6/7	Oi/Ase	AS	2.5Y 2.5/1	nd	gr/1/f	VF			N	3/f	S/ST
	6/7 - 15	Ase	CS	10YR 2/2	SaL	gr/1/f	MF			N	2/f	S/ST
	15 - 20	A/Cse	CS	5Y 52.5/2	Sa	sg/0	VF			N	1/m	S/ST
	20 - 31	Cse	CS	5Y 3/1	Sa	sg/0	VF	F3M/c/3/P	5Y 2.5/2	N	1/vf	S/ST
	31 - 50+	Cg	-	Gley1 3/10Y	Sa	sg/0	VF	OSF/c/3/D	Gley1 2.5/10Y	N	1/f	S/SM
CER	0 - 5	Ase	CW	Gley1 2.5/5GY	SiL	pl/1/f	VF			Y		S/ST
	5 - 10	Ag	CW	Gley1 4/10Y	SiL	pl/1/m	SF	F2M/c/2/P	Gley1 3/5GY	Y	1/vf	S/SM
	10 - 23	Cse	AW	Gley1 3/5GY	SiCL	pl/1/m	SF	F2M/m/3/P	Gley2 2.5/5PB	Y	1/vf	S/SM
	23 -35	2Cse	-	Gley1 3/N	LSa	sg/0	MF	F2M/m/4/P	Gley1 2.5/N	Y		S/ST
PA	0 - 4	Ase	CW	5Y 2.5/1	SiL	gr/1/m	VF	OSF/m/1/D	5Y 3/1	Y	2/f	S/SM
	4 - 10	Ag	AW	5Y 3/1	SiL	gr/1/m	MF	OSF/m/1/D	5Y 2.5/1	Y	1/f	S/SL
	10 - 17	Cg1	AW	5Y 4/1	SiCL	sbk/2/f	SF	F3M/c/3/P	5Y 4/2	Y	1/f	S/SL
	17 - 32+	Cg2	-	5Y 5/1	SiCL	sbk/2/f	SF	F3M/m/3/P	5Y 5/3; 2.5Y 5/4	Y		S/SL

Horizon master: se = presence of sulfide; g = gleying. **Horizon boundary:** (D) Distinctness: A = abrupt, C = clear, G = gradual, D = diffuse / (T) Topography: S = smooth, W = wavy, I = irregular, U = unknown; **Field texture class:** Sa = sand, SaL = Sandy Loam, L = Loam, LSa = Loamy Sand, SiL = Silty Loam; SiCL = Silty Clay Loam; **Structure:** (T) Type: gr = granular, abk = angular blocky, sbk = subangular blocky, pl = platy, sg = single grain / (G) Grade: 0 = structureless, 1 = weak, 2 = moderate / (S) Size: vf = very fine, f = fine, m = medium; **Fluidity classes:** SF = Slightly Fluid, MF = Moderately Fluid, VF = Very Fluid; **Mottles/redoximorphic features (RMFs):** (K) Kind: F2M = reduced iron, F3M = oxidated iron, OSF = organic stains / (Q) Quantity: f = few, c = common, m = many / (S) size: 1 = fine, 2 = medium, 3 = coarse, 4 = very coarse, 5 = extremely coarse / (Sh) Shape: D = dendritic, P = platy; **Roots:** (Q) Quantity: 1 = few, 2 = common, 3 = many / (S) Size: vf= very fine, f = fine, m = medium, co = coarse; **Odor:** (K) Kind: N = none, S = sulfurous / (I) Intensity: SL= slight, MD= moderate, ST= strong.

Tab. S2 – Table reporting different diversity indeces for the three sites. S=total taxa richeness; J= Pielou's index; H= Shannon's index.

		PA	CER	PIR
S	Mean	2690.5	2920.67	2742.67
	St.Dev	140.5	56.41	193.77
	Min	2550	2841	2481
	Max	2831	2964	2944
J'	Mean	0.96	0.96	0.95
	St.Dev	0	0	0.01
	Min	0.95	0.96	0.94
	Max	0.96	0.96	0.96
H	Mean	7.57	7.66	7.52
	St.Dev	0.09	0.02	0.12
	Min	7.48	7.63	7.36
	Max	7.65	7.68	7.65

Tab. S3 - Results of ANOVA analysis testing difference in : total taxa richness (S between sites). Df = Degress of Freedom; Sum.Sq = Sum of Squares; Mean Sq.= Mean Square; Pseudo F = pseudo-F statistic; P (perm)= Permutation test .

S	**df**	**SS**	**MS**	**Pseudo-F**	**P(perm)**
Site	2	77418	38709	1.1972	0.3341
Res	5	1.6167E+05	32334		
Total	7	2.3909E+05			

Tab.S4 - Results of ANOVA analysis testing difference in Pielou's index (J).between sites. Df = Degress of Freedom; Sum.Sq = Sum of Squares; Mean Sq.= Mean Square; Pseudo F = pseudo-F statistic; P (perm)= Permutation test .

J	**df**	**SS**	**MS**	**Pseudo-F**	**P(perm)**
Site	2	0.00013921	6.9604E-05	1.8722	0.1853
Res	5	0.00018589	3.7177E-05		
Total	7	0.0003251			

Tab.S5 - Results of ANOVA analysis testing difference in Shannon's index (H.between sites. Df = Degress of Freedom; Sum.Sq = Sum of Squares; Mean Sq.= Mean Square; Pseudo F = pseudo-F statistic; P (perm)= Permutation test .

H	**df**	**SS**	**MS**	**Pseudo-F**	**P(perm)**
Site	2	0.028593	0.014297	1.1586	0.3506
Res	5	0.061699	0.01234		
Total	7	0.090292			

Tab. S6– Results of Permanova results testing differences among the three study sites

	Df	SumOfSqs	R2	F	Pr(>F)
permanova_var$Group	2	0.354333	0.54102	2.946866	0.0043
Residual	5	0.300602	0.45898	NA	NA
Total	7	0.654934	1	NA	NA

Tab. S7– References used to identify ecological functions of most abundant genus

Genus	Function	Reference	DOI
Thiobacillus	Sulfur oxidation	Haaijer et al., 2007	10.1080/01490450701436489
Sulfovorum	Sulfur oxidation	Sharma et al., 2020	10.1186/s12866-020-01923-3
Sulfuricurvum	Sulfur oxidation	Cron B et al., 2019	10.3389/fmicb.2019.02710
Desulfatiglans	Sulfate reduction	Galushko et al., 2019	https://doi.org/10.1002/9781118960608.gbm01679
Desulfosarcina	Sulfate reduction	Watanabe et al., 2020	https://doi.org/10.1002/9781118960608.gbm01020.pub2
Desulforomonas	Sulfate reduction	Widdel et al. 1992	https://doi.org/10.1007/978-1-4757-2191-1_22
Syntrophus	Syntrophic relationships	Galushko et al., 2019	https://doi.org/10.1002/9781118960608.gbm01064.pub2